# Influence of the characteristics of the 3D FE mesh on the evolution of variables used to characterize the stress state

Cite as: AIP Conference Proceedings **2113**, 160015 (2019); https://doi.org/10.1063/1.5112712
Published Online: 02 July 2019

J. P. Brito, M. C. Oliveira, D. M. Neto, J. L. Alves, and L. F. Menezes

# Influence of the Characteristics of the 3D FE Mesh on the Evolution of Variables Used to Characterize the Stress State

J.P. Brito[1, a)], M.C. Oliveira[1, b)], D.M. Neto[1, c)], J.L. Alves[2, d)] and L.F. Menezes[1, e)]

[1]*CEMMPRE, Department of Mechanical Engineering, University of Coimbra, Pólo II, Rua Luís Reis Santos, Pinhal de Marrocos, 3030-788 Coimbra, Portugal*
[2]*CMEMS, Department of Mechanical Engineering, University of Minho, Campus de Azurém, 4800-058 Guimarães, Portugal*

[a)]joao.brito@uc.pt
[b)]Corresponding author: marta.oliveira@dem.uc.pt
[c)]diogo.neto@dem.uc.pt
[d)]jlalves@dem.uminho.pt
[e)]luis.menezes@dem.uc.pt

**Abstract.** It is well-established that the ductile fracture in metallic materials is a highly stress state dependent physical process. Past research has focused on the development of numerical tools that describe the mechanisms of the ductile damage. In this framework, the computed damage distribution is affected by the accuracy in the description of the stress state history, aside from the choice of the damage model. Thus, the main objective of this work is to assess the influence of the discretization adopted in the gauge area of fracture-calibration specimens, in the evolution and distribution of the field variables generally used to describe the stress state: the stress triaxiality and the Lode parameter. The numerical analysis is performed with the in-house solver DD3IMP. The results show that the required mesh refinement changes particularly when plastic instabilities arise. Moreover, the stress state variables can present an heterogenous distribution at the integration point level, which is in general smoothed when analysing the results at the nodes.

## INTRODUCTION

The evaluation of formability of thin-walled components still represents a non-trivial issue in sheet metal forming process. Past research has focused on the development of numerical tools that describe internal damaging and, ultimately, fracture of ductile materials, which is known to be strongly dependent on the stress state [1]. In this context, damage models must be able to capture the characteristic load-path dependent failure behaviour and provide a reliable prediction of the stress and strain histories. Thus, damage models establish the link between field variables (e.g. stress tensor, stress triaxiality) and the progressive deterioration towards fracture. One way of achieving this connection is by the so-called uncoupled models, which employ conventional plasticity models together with a damage indicator to predict ductile fracture. In other words, a conventional finite element (FE) simulation is carried out and the damage is evaluated exclusively as a post-processing step of the FE solution. The damage accumulation is formulated empirically or semi-empirically through a scalar internal variable $D$, with the general criterion:

$$D = \int_0^{\bar{\varepsilon}_f^p} f(\boldsymbol{\sigma}, \boldsymbol{\varepsilon}^p)\, d\bar{\varepsilon}^p \geq D_c, \tag{1}$$

where $\bar{\varepsilon}^p$ is the equivalent plastic strain, $\bar{\varepsilon}_f^p$ is the critical value of equivalent plastic strain at fracture for a given loading path, $\boldsymbol{\sigma}$ is the Cauchy stress tensor and $\boldsymbol{\varepsilon}^p$ is the plastic strain tensor. The integrand $f(\boldsymbol{\sigma}, \boldsymbol{\varepsilon}^p)$, is the weighting function of damage and represents a general function of the field variables. Fracture is considered to occur when the damage indicator $D$, computed at the integration point (in this work, Gauss point (GP)) of the FE model, exceeds a critical damage value, $D_c$.

*Proceedings of the 22nd International ESAFORM Conference on Material Forming*
AIP Conf. Proc. 2113, 160015-1–160015-6; https://doi.org/10.1063/1.5112712
Published by AIP Publishing. 978-0-7354-1847-9/$30.00

The stress state is usually described by two dimensionless parameters: the stress triaxiality, $\eta$, and the Lode angle parameter, $\bar{\theta}_{\mathrm{L}}$. Let $I_1$ denote the first invariant of the Cauchy stress tensor, $\boldsymbol{\sigma}$, and $J_2, J_3$ the second and third invariants of the deviatoric stress tensor, $\boldsymbol{\sigma}'$, respectively. Hence, one can write:

$$I_1 = \mathrm{tr}(\boldsymbol{\sigma}), \quad J_2 = \frac{1}{2}\boldsymbol{\sigma}' : \boldsymbol{\sigma}', \quad J_3 = \det(\boldsymbol{\sigma}'), \quad \text{with } \boldsymbol{\sigma}' = \boldsymbol{\sigma} - \frac{1}{3}\mathrm{tr}(\boldsymbol{\sigma})\mathbf{I}, \tag{2}$$

$$\eta = \frac{1}{3}\frac{I_1}{\sqrt{3J_2}} = \frac{\sigma_{\mathrm{m}}}{\bar{\sigma}_{\mathrm{Mises}}}, \quad \text{where } \sigma_{\mathrm{m}} = \frac{1}{3}I_1 \text{ and } \bar{\sigma}_{\mathrm{Mises}} = \sqrt{3J_2}, \tag{3}$$

$$\bar{\theta}_{\mathrm{L}} = \left(1 - \frac{2}{\pi}\arccos(\xi)\right) = \frac{2}{\pi}\arcsin(\varphi), \quad \text{with } \varphi = \frac{3\sqrt{3}}{2}\frac{J_3}{(J_2)^{3/2}}. \tag{4}$$

$\sigma_{\mathrm{m}}$ is the mean stress and $\varphi$ is the normalized $J_3$. The Lode angle can be understood as a quantification of the proximity (or remoteness) of a stress state relative to the pure-shear stress state. Its effect on the material damaging is less intuitive, but recent studies indicate that it can be as important as the stress triaxiality on the equivalent strain to fracture [1]. Any loading path can be defined by the pair $(\eta, \bar{\theta}_{\mathrm{L}})$. Note that a third independent parameter (e.g. a stress invariant) is required to set the magnitude of the stress state and thus fully define it.

Analysing Eq. (1), one can argue that the correct prediction of the accumulated damage is inherently related to the reliable computation of the field variable distributions that integrate the weighting function, $f(\boldsymbol{\sigma}, \boldsymbol{\varepsilon}^{\mathrm{p}})$. Thus, the main goal of the present work is to analyse the influence of the discretization adopted in the gauge area of test specimens, commonly used to calibrate ductile fracture models, in the evolution and distribution of the field variables $(\eta, \bar{\theta}_{\mathrm{L}})$. Two stress states, i.e. $(\eta, \bar{\theta}_{\mathrm{L}})$ combinations, of great importance to the sheet metal forming process are targeted: (i) uniaxial tension – $(1/3, 1)$; and (ii) simple shear – $(0, 0)$.

# NUMERICAL MODEL

## Plasticity Model

The numerical tests performed in the present work consider a 1 mm thick dual phase steel DP780. According to Abedini et al. [2] this material displays relatively isotropic mechanical properties. Therefore, the yield of the material is described using the isotropic von Mises criterion:

$$\Phi(\boldsymbol{\sigma}, \bar{\varepsilon}_{\mathrm{p}}) = \bar{\sigma}_{\mathrm{Mises}} - Y(\bar{\varepsilon}_{\mathrm{p}}) = 0, \quad \text{with } \bar{\sigma}_{\mathrm{Mises}} = \sqrt{\frac{3}{2}\boldsymbol{\sigma}' : \boldsymbol{\sigma}'}, \tag{5}$$

and an associated flow rule is adopted. $\bar{\varepsilon}_{\mathrm{p}}$ is the equivalent plastic strain, defined as work-conjugate of the von Mises equivalent stress, $\bar{\sigma}_{\mathrm{Mises}}$. $Y(\bar{\varepsilon}_{\mathrm{p}})$ denotes the flow stress that is modelled through a combined Swift-Voce isotropic hardening law, as follows:

$$Y(\bar{\varepsilon}_{\mathrm{p}}) = \alpha Y_{\mathrm{Swift}}(\bar{\varepsilon}_{\mathrm{p}}) + (1-\alpha) Y_{\mathrm{Voce}}(\bar{\varepsilon}_{\mathrm{p}}), \quad \text{with} \quad \begin{array}{l} Y_{\mathrm{Swift}}(\bar{\varepsilon}_{\mathrm{p}}) = K(\varepsilon_0 + \bar{\varepsilon}_{\mathrm{p}})^n, \\ Y_{\mathrm{Voce}}(\bar{\varepsilon}_{\mathrm{p}}) = Y_0 + (Y_{\mathrm{sat}} - Y_0)\left(1 - e^{-C_{\mathrm{Y}}\bar{\varepsilon}_{\mathrm{p}}}\right), \end{array} \tag{6}$$

in which $\alpha$ is a linear weighting factor, $\{K, \varepsilon_0, n\}$ are the Swift law parameters and $\{Y_0, Y_{\mathrm{sat}}, C_{\mathrm{Y}}\}$ are the Voce law parameters. The elastic behaviour is assumed isotropic and constant, described by the Hooke's law parameters $\{E, \nu\}$. The required material parameters have been identified by Roth and Mohr [3] and are summarized in Table 1.

## Specimen Geometries and Discretization

The uniaxial tension stress state is achieved using a standard flat tensile specimen. Due to material and geometrical symmetry conditions, only one eighth of the tensile specimen is modelled. The relevant model dimensions and the coordinate system adopted are presented in Fig. 1. The specimen grip section is also modelled such that the displacement of the nodes contained in the grip free surface are constrained, except in the axial direction, for which a displacement of $u_x = 5.1$ mm is prescribed. This ensures that the initial stress and strain fields are fully homogeneous in the gauge section until the triggering of the initiation of localized necking. Concerning the simple shear stress state, Peirs et al. [4] shear specimen is adopted, which was designed such that an applied tensile load originates a shear stress in its gauge section, located in the centre of the specimen. The geometry and relevant dimensions of this flat specimen are shown in Fig. 2. The eccentric position of the notches intend to maintain a hypothetical zero stress

**TABLE 1.** Elastic properties and combined Swift-Voce hardening law parameters of the DP780 steels (as in Roth and Mohr [3]).

| **Elastic Properties** | | **Voce Law** | | | **Swift Law** | | | **Combined Law** |
|---|---|---|---|---|---|---|---|---|
| $E$ [GPa] | $\nu$ [-] | $Y_0$ [MPa] | $Y_{sat}$ [MPa] | $C_Y$ [-] | $K$ [MPa] | $\varepsilon_0$ [-] | $n$ [-] | $\alpha$ [-] |
| 194 | 0.33 | 349.54 | 885.9 | 93.07 | 1315.4 | $0.28 \cdot 10^{-4}$ | 0.146 | 0.7 |

triaxiality stress state up to large strains. Exploiting the symmetry of the specimen geometry only half of its thickness is modelled. A fixed boundary condition is applied at the lower-end of the grip, and a total displacement of $u_x = 1.4$ mm along the $x$-direction (see Fig. 2), is prescribed at the opposite end.

Regarding the FE discretization, the gauge sections of both specimens are discretized with structured and regular meshes. Since the area surrounding the gauge section undergoes very small plastic strain, this zone is discretized with a coarse and unstructured mesh. Given the different length scale of the studied specimens, the average finite element size, $l_{elem}$, is defined according to the dimensionless parameter $\mu = (l_{elem}/l_{char})$, such that the adopted in-plane mesh refinement is equivalent for both numerical tests. For the tensile specimen, the characteristic dimension, $l_{char}$, selected corresponds to the smallest dimension of the gauge section, i.e. its width, $w_0$ (see Fig. 1). As for the shear specimen, the characteristic dimension is the gauge section length, $l$, (see Fig. 2). Three in-plane (P) mesh discretizations are considered, corresponding to $\mu$ values of 20, 40 and 100. Additionally, three discretizations along the sheet thickness direction are employed, corresponding to 2, 4 and 8 layers (L). Thus, four FE meshes are generated combining the previous in-plane and through-thickness discretizations, labelled by: P020L2, P040L4, P100L4 and P100L8. All meshes comprise eight-node hexahedral solid finite elements and a selective reduced integration (SRI) technique is employed, with eight and a single GP for the deviatoric and hydrostatic parts of the velocity field gradient, respectively. The main characteristics of the adopted meshes are summarized in Table 2, as well as the respective computational requirements, quantified by the total elapsed CPU time[1]. The simulations are performed with the in-house quasi-static elastoplastic fully implicit finite element solver DD3IMP, specifically developed to simulate sheet metal forming processes [5,6].

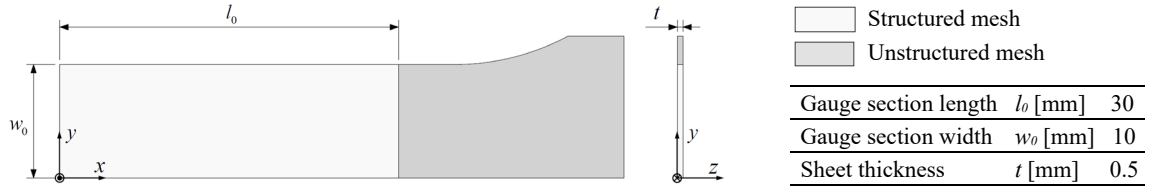


**FIGURE 1.** Dimensions of the modelled tensile specimen gauge section. Delimitation of the structured and unstructured zones.

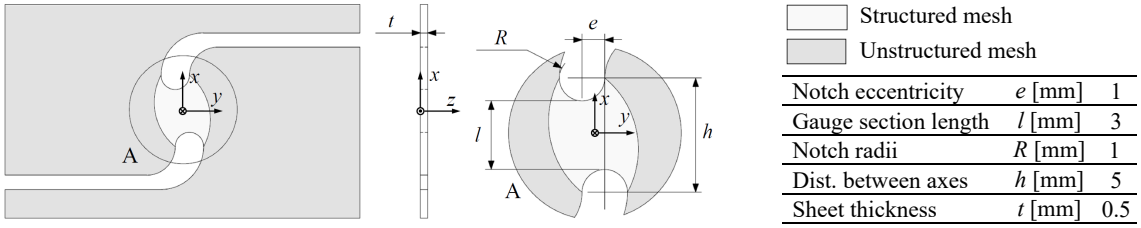


**FIGURE 2.** Dimensions of Peirs et al. [4] specimen gauge section. Delimitation of the structured and unstructured zones.

**TABLE 2.** Mesh characteristics and corresponding computational time for the finite element simulations.

| **Mesh** | **Tensile specimen** | | | **Shear specimen** | | |
|---|---|---|---|---|---|---|
| | # Elements | # Nodes | CPU time [h] | # Elements | # Nodes | CPU time [h] |
| P020L2 | 2728 | 4380 | 0.02 (42 Steps) | 3438 | 5502 | 0.01 (42 Steps) |
| P040L4 | 20212 | 26105 | 0.20 (49 Steps) | 20032 | 25775 | 0.06 (42 Steps) |
| P100L4 | 122004 | 154410 | 1.69 (56 Steps) | 109788 | 138420 | 0.46 (44 Steps) |
| P100L8 | 244008 | 277938 | 8.59 (58 Steps) | 219576 | 249156 | 2.16 (46 Steps) |

[1] All numerical simulations are carried on a single computer machine equipped with an Intel® Core™ i7-8700K (6C/12T) @ 3.70 GHz base frequency processor with 2x8GB DDR4 @ 2400 MHz CL17 memory kit on a 64-bit Windows 10 Pro for Workstations operating system.

## RESULTS AND DISCUSSION

The computed force-displacement curves, along with the evolution of the equivalent plastic strain (EPS) at the GP closest to the origin of the studied specimens, are depicted in Fig. 3. Regarding the tensile specimen (see Fig. 3a), it is verified that, until diffuse necking occurs – i.e. a maximum axial load is reached, the FE discretization has little influence on the numerical results. Past this point, localized necking is reached, (manifested by severe thinning on a narrow diagonal band), and a fully three-dimensional stress state arises. Given the resultant high strain gradients, the FE results become sensitive to mesh refinement, and, thus, very fine meshes are needed to reliably compute the stress and strain distributions. This ultimately justifies the divergence of the plotted global and local variables in Fig. 3a, at the end of the simulation. Note that the more refined the FE mesh, the greater is the predicted ultimate EPS. The force-displacement evolutions for the shear specimen tests show a very distinct behaviour. Since no through-thickness necking occurs, the strain distribution in the gauge section is much more homogeneous during the entire deformation process. Hence, both the computed force and EPS are less sensitive to the mesh refinement.

Figure 4 shows the evolution of the studied field variables, $(\eta, \bar{\theta}_L)$. The same observations hold true for this case, i.e. since necking only takes place in the tensile test, the stress triaxiality and the Lode parameter are shown to be more sensitive to the mesh refinement. Note that prior to necking, the evolution of both parameters coincide with their theoretical values, regardless of the discretization. On the contrary, for the shear specimen, despite the similar results regarding the mesh refinement, the stress state parameters $(\eta, \bar{\theta}_L)$ vary during the entire deformation process around the theoretical values for a pure-shear stress state. Note that adding an additional 4 layers to the finest in-plane mesh (P100) does not considerably improve the numerical results, even for the tensile test, for which a through-thickness strain gradient appears after necking.

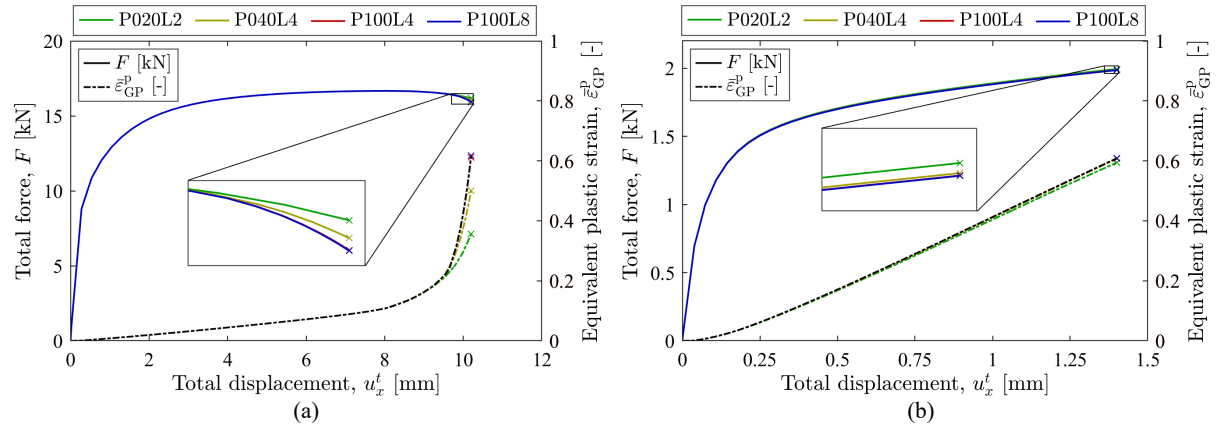


**FIGURE 3.** Influence of the FE mesh on the force-displacement evolution (global variable) and on the equivalent plastic strain evolution (local variable) for the: (a) tensile specimen; (b) shear specimen.

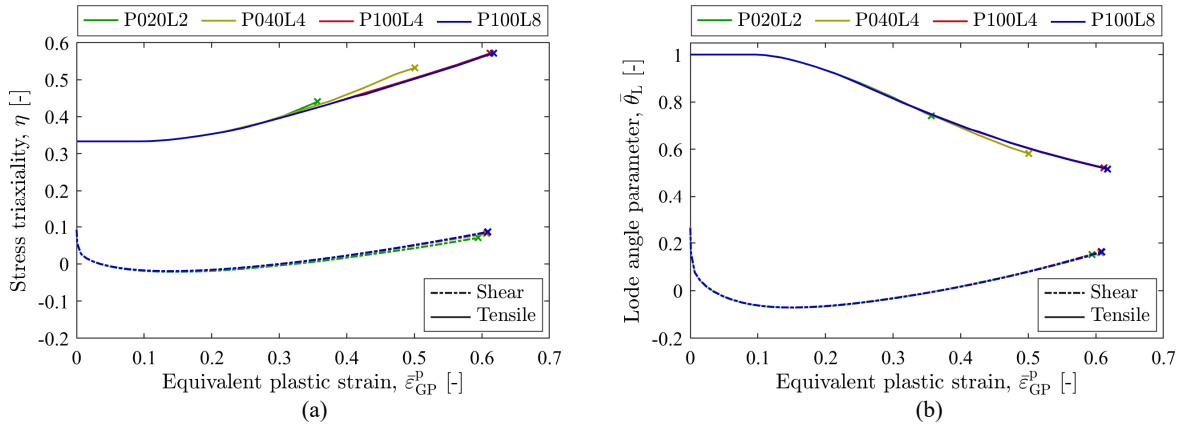


**FIGURE 4.** Influence of the FE mesh on the evolution of the field variables: (a) stress triaxiality; (b) Lode angle parameter, for both specimens. The data is evaluated at the GP closest to the specimen's coordinate system origin.

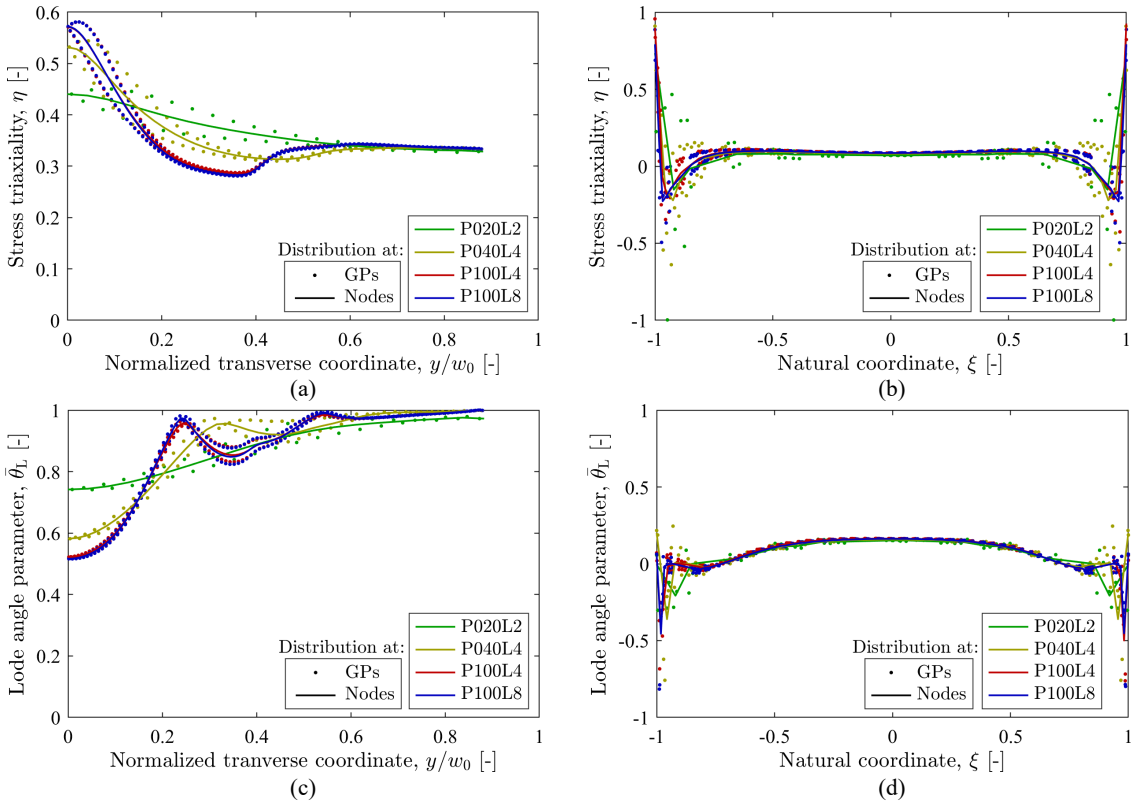


**FIGURE 5.** Influence of the FE mesh on the distribution of the stress triaxiality for: (a) tensile specimen; (b) shear specimen; and the Lode angle parameter distribution for: (c) tensile specimen; (d) shear specimen. Data evaluated at the final simulation step.

Figure 5 shows the distribution of the stress state parameters $(\eta, \bar{\theta}_L)$ at the final instant of the deformation process, for both specimens. The distributions are evaluated at the GPs and at the nodes of the FE model (unweighted arithmetic mean of the neighbouring GPs values), along a given direction. For the tensile specimen, the transverse direction, normalized by its initial width, $y/w_0$, is chosen. As for the shear specimen, the distribution is evaluated along a natural coordinate, $\xi$, collinear with the axis on which a narrow strain band arises, as shown in Fig. 6a.

Figure 5a and Fig. 5c clearly corroborate that the prediction of the post-necking distribution of the field variables $(\eta, \bar{\theta}_L)$ requires finer discretizations. Indeed, the finer the mesh, the greater the detail in which the field variable gradients are captured. Regarding the shear specimen, given the absence of a plastic instability, the distribution of $(\eta, \bar{\theta}_L)$ at the centre of the gauge section is independent of the mesh refinement. The sensitivity to the discretization is recovered only at the gauge section border, where, as shown in Fig. 6b, there is an abrupt change of the stress state due to the free-boundary effects.

Concerning the distribution of the parameters $(\eta, \bar{\theta}_L)$ at the GPs, there is a departure from the results at the nodes – that is, the respective trend line – takes place in both specimens. In other words, significant oscillations of the results at the GPs are computed, both between adjacent FE and within a FE itself. Note that these discontinuities do not vanish with the mesh refinement and their amplitude vary throughout the domain of Fig. 5. In order to analyse the source of these unstable distributions, Fig. 7a and Fig. 7b show the distribution of the pair of invariants that define the stress state parameters $(\eta, \bar{\theta}_L)$ (see Eq. (3) and Eq. (4), respectively), at the final instant of the tensile test. Analysing Fig. 7 it is clear that the oscillations of the stress triaxiality and the Lode angle parameter are exclusively due to the unstable distribution of the mean stress (i.e. $I_1$ - invariant) and the $J_3$ - invariant, respectively. Indeed, the von Mises equivalent stress (i.e. $J_2$ - invariant) does not show any kind of oscillation.

As a result of the non-uniform computation of the field variables $(\eta, \bar{\theta}_L)$ at the GPs, uncoupled damage models may predict a highly local and equally discontinuous damage distribution at the GPs, which could lead to a somewhat misleading prediction of fracture. The evaluation of the FE results only at the nodes, i.e. in a smoothed way, can conceal problems of excessive heterogeneity of the distribution of local variables such as $(\eta, \bar{\theta}_L)$ and, ultimately, of the ductile damage, $D$.

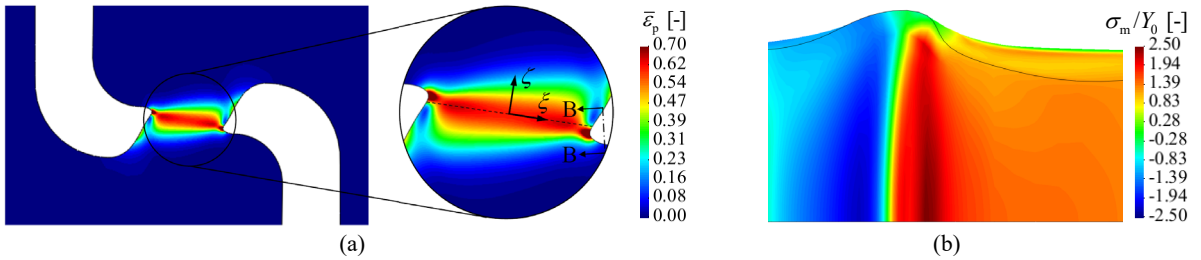


(a) (b)

**FIGURE 6.** Contour plots of the shear specimen at the final simulation step: (a) Equivalent plastic strain; (b) normalized mean stress (at section B-B). Note the localized band within the gauge section and the thickening along the free-boundary.

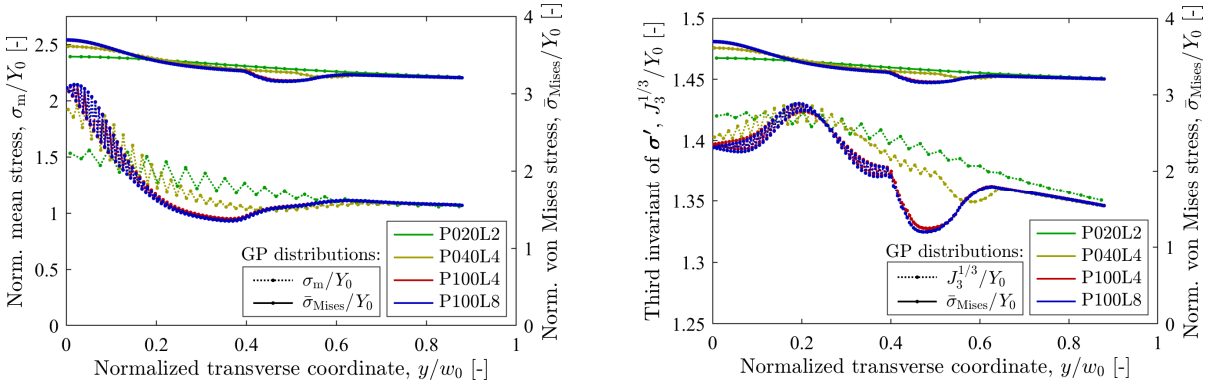


(a) (b)

**FIGURE 7.** Tensile specimen's final distribution at the Gauss points (GP) of the: (a) normalized mean stress; (b) third invariant of the deviatoric stress tensor. For comparison, the normalized von Mises equivalent stress is equally represented.

## CONCLUSIONS

In this work, a FE analysis is performed in order to assess the mesh-sensibility of the evolution and distribution of two field variables: the stress triaxiality and the Lode angle parameter. For this purpose, two fracture-characterization specimens are studied, namely, a flat tensile specimen and a flat simple shear specimen, proposed by Peirs et al. [4].

The results show that the required mesh refinement changes particularly when plastic instability occurs. The field variable distribution at the GPs shows that non-negligible oscillations can arise relative to the smoothed results at the nodes. Since, within damage models, the internal damage variable is computed at the GP level, an excessively heterogeneous distribution of the field variables may equally lead to a discontinuous damage distribution.

## ACKNOWLEDGMENTS

The authors gratefully acknowledge the financial support of the Portuguese Foundation for Science and Technology (FCT) under the projects with reference PTDC/EMS-TEC/0702/2014 (POCI-01-0145-FEDER-016779), PTDC/EMS-TEC/6400/2014 (POCI-01-0145-FEDER-016876) and PTDC/EME-EME/30592/2017 (POCI-01-0145-FEDER-030592) and by UE/FEDER through the program COMPETE2020 under the project MATIS (CENTRO-01-0145-FEDER-000014).

## REFERENCES

[1] C. C. Roth and D. Mohr, *Int. J. Mech. Sci.*, **149**, 224–240 (2018).
[2] A. Abedini, C. Butcher, D. Anderson, M. Worswick, and T. Skszek, *SAE Int. J. Mater. Manuf.*, **8**, 774-782 (2015).
[3] C. C. Roth and D. Mohr, *Int. J. Plast.*, **79**, 328–354 (2016).
[4] J. Peirs, P. Verleysen, and J. Degrieck, *Exp. Mech.*, **52**, 729–741 (2012).
[5] L. F. Menezes and C. Teodosiu, *J. Mater. Process. Technol.*, **97**, 100–106 (2000).
[6] M. C. Oliveira, J. L. Alves, and L. F. Menezes, *Arch. Comput. Methods Eng.*, **15**, 113–162, (2008).